Advances in Nano Research, *Vol. 19, No. 1 (2025) 75-89*
https://doi.org/10.12989/anr.2025.19.1.075

Electronic and optical properties of WS2(6,6)@MoS2(14,14) and WS2(8,8)@MoS2 (16,16) van der Waals nanotubes under the influence of an external electric field

Daulet Sergeyev*[1,2], Assemay Kenges[1] and Kuanyshbek Shunkeyev[1]

[1]Department of Physics, K. Zhubanov Aktobe Regional University, 34A Moldagulova avenue, 030000 Aktobe, Kazakhstan
[2]Department of Radio Electronics, T. Begeldinov Aktobe Aviation Institute, 39 Moldagulova avenue, 030012 Aktobe, Kazakhstan

(*Received March 10, 2025, Revised May 16, 2025, Accepted July 7, 2025*)

Abstract. One-dimensional nanostructures based on transition metal dichalcogenides (TMDs) have attracted considerable attention for applications in next-generation quantum devices. However, the influence of external factors on their electronic and optical properties remains insufficiently understood. In this study, the effects of an external electric field on the electronic and optical properties of 1D van der Waals (vdW) heterostructures WS_2(6,6)@MoS_2(14,14) and WS_2(8,8)@MoS_2(16,16) were investigated within the framework of density functional theory (DFT) using the GGA-PBE approximation. The electronic band structures, complex dielectric functions, absorption coefficients, and refractive indices were computed. The results show that with increasing external electric field strength: the band gap of the vdW heterostructures WS_2(6,6)@MoS_2(14,14) and WS_2(8,8)@MoS_2(16,16) decreases, and a semiconductor-to-metal transition occurs at field strengths of 16 V and 18 V, respectively; the values of static dielectric permittivity increase due to charge redistribution; the amplitude of the absorption coefficient peak decreases and shifts to the low-energy region as a result of charge redistribution and enhanced ionic polarizability.

Keywords: absorption coefficient; bandgap; complex dielectric function; molybdenum disulfide MoS_2; one-dimensional van der Waals nanostructures; refractive index; transition metal dichalcogenide nanotubes; tungsten disulfide WS_2

1. Introduction

Recently, one-dimensional nanostructures (nanotubes) have attracted great interest due to their unique physico-chemical properties, mainly dependent on their diameter and chirality (Li *et al*. 2024, Hatakeyama *et al*. 2024, Dhanasekaran *et al*. 2025, Sergeyev 2020a). However, synthesizing nanotubes with a specific chirality is a very challenging task (Kharlamova 2023), which leads to a decreased probability of reproducing the unique properties of nanotubes with the slightest inaccuracy. Therefore, various other approaches for controlling the electronic properties of nanotubes are currently being considered. One of them is filling the inner cavity of nanotubes with metallic (Kharlamova and Kramberger 2023) and semiconducting structures (Jin *et al*. 2021). It is important to mention that introducing an electron donor (with a Fermi level located in the conduction band of the nanotubes) into the channels of metallic nanotubes can lead to an increase in the electron density on its walls, which will manifest itself in an increase in its conductivity. Introducing an electron acceptor (with a Fermi level below the Fermi level of the nanotube) can cause the system to transition into a semiconducting state. Thus, the encapsulation of electron donor or acceptor substances inside a single-walled carbon nanotube leads to a significant shift in the Fermi level (Kharlamova and Kramberger 2022).

Filling the inner channel strengthens nanotubes in the radial direction, while simultaneously combining the properties of both the host (CNTs) and the guest fillers (Poudel *et al*. 2023, Jayakumari *et al*. 2024). At present, the technology for producing metal-filled nanotubes is being actively employed in the fabrication of nanowires and metal-organic frameworks (Qiu *et al*. 2021). Interesting results have been obtained in the study of the mechanical and electrical properties of CNTs filled with copper. The electrical resistance of composite wires made of double-walled CNTs and copper, fabricated using a combination of spark plasma sintering and wire drawing at room temperature, increases by 12% (at 77 K) compared to pure copper wires, and their tensile strength increases by ~10% (Arnaud *et al*. 2016, Bazbouz *et al*. 2021). Notably, one should consider that filling the inner channel of CNTs with silicon can produce an anode material for lithium-ion batteries with improved capacity (Guo *et al*. 2024), and CNTs with a titanium dioxide filler can be used for water purification and for the development of solar cells with high efficiency (Akhter *et al*. 2024, Liang *et al*. 2022).

One important class of nanotubes with filled channels is multi-walled carbon nanotubes (MWCNTs) (Chaudhary and Singh 2021, Yin *et al*. 2021). Such nano-objects are telescopically (coaxially) superimposed on each other with different diameters of CNTs (homostructures). In such nanosystems, inter-shell interactions play a key role in structural stability and influence their electronic properties. The inter-shell transport of quasiparticles in coaxial nanosystems is analogous to electron transport through molecules, in the sense that both processes occur within

---

*Corresponding author, Professor,
E-mail: serdau82@gmail.com

http://www.techno-press.org/?journal=journal=anr&subpage=5
ISSN: 2287-237X (Print), 2287-2388 (Online)

spatially confined regions. In (Park *et al*. 2023), such coaxial CNTs in the form of hybrid composites (Bi_2S_3-SnS_2-MWCNT) were employed in the development of thermoelectric converters with high energy conversion efficiency. Recently, within the framework of density functional theory combined with the non-equilibrium Green's function method (DFT+NEGF), we have investigated the electron transport properties of a one-dimensional nanodevice consisting of telescopic polyprismanes with different types of electrical conductivity (Sergeyev 2021). It was shown that the bandgap width and electron transport strongly depend on the diameter of the polyprismane devices.

Another approach to controlling the electronic properties of nanotubes is filling their internal channel with another type of nanotube with a smaller diameter. In this case, these nanotubes are connected to each other by weak van der Waals forces, i.e., they form one-dimensional van der Waals nanoheterostructures (Guo *et al*. 2025, Cambre *et al*. 2021, Wang *et al*. 2021, Xiang *et al*. 2020, Mohammed *et al*. 2024). One should take into account that compared to two-dimensional ones, one-dimensional vdW heterostructures are strongly limited in radial size, and the atoms of such structures are also in a stressed state due to the radial shape. Such spatial constraints enhance the properties of one-dimensional heterostructures, such as the transfer of electrons (or photons) in the radial direction (Feng *et al*. 2021).

One of the promising materials for the development of unique one-dimensional nanostructures are transition metal dichalcogenides (TMDs) (MeX_2, where Me = Mo, W, Nb, V, Ta, Ti), X – chalcogen (sulfur, selenium)) (Baithi and Duong 2024, Moon 2024, Rasulov *et al*. 2024, Sergeyev and Duisenova 2021, Kumar and Benazir 2024). Notably, TMD-based nanostructures, for example, NbS_2, $NbSe_2$, TaS_2, $TaSe_2$, have superconducting properties (Sinko *et al*. 2021, Ding *et al*. 2022), and interesting effects related to the phenomenon of superconductivity manifest themselves in them at low temperatures below the critical temperature (Tsuppayakorn-aek *et al*. 2021, Sergeyev *et al*. 2024a).

TMD-based nanotubes have a wide range of electronic properties, acting as metals, semimetals, semiconductors with varying band gap widths, or dielectrics (Liu *et al*. 2021). With the appropriate sequence and combination of TMD-1D structures, it is possible to obtain ultra-miniature semiconductor-metal heterojunctions, as well as electron-hole junctions and sensors a few nanometers in size. However, despite the bouquet of exciting quantum properties of one-dimensional nanoheterostructures, it should be noted that the technology for experimentally obtaining such nanoheterostructures is still in its infancy (Guo *et al*. 2022). We believe that improving the technology for obtaining one-dimensional nanoheterostructures is inevitable. The synthesis of such 1D heterostructures has already been proposed by folding quasi-two-dimensional layered TMDs, for example, MoS_2/WS_2, as well as compositionally-selective and phase-selective methods for manufacturing low-dimensional TMD compounds (Kim *et al*. 2020). Currently, the synthesis technology of low-dimensional TMDs is being intensively developed, since it is possible to create ultra-miniature field-effect transistors, sensors, LEDs, photodetectors (including materials for solar cells) and other nanodevices based on the quantum properties of 1D and 2D vdW nanoheterostructures (Matsushita *et al*. 2023, Zhu *et al*. 2021, Yang *et al*. 2021).

Of particular interest is the study of charge carrier transport in TMD nanotubes under the influence of an electric field. It is known that in TMD nanotubes, due to their quasi-one-dimensionality and the short length of defect zones, charge carriers can travel long distances without scattering. Moreover, the application of an electric field accelerates carriers while minimizing their interaction with phonons and defects. In the work (Xie *et al*. 2024), the charge carrier transport in $BC_6N/MoSe_2$ nanoheterostructures under the influence of an electric field was studied, and it was shown that the band gap linearly decreased with increasing electric field intensity.

In recent years, first-principles methods have been widely employed for the theoretical investigation of the electronic and optical properties of TMD-based heterostructures. The concept of first-principles calculations for studying the electronic and optical behavior of TMD nanostructures serves as a powerful tool for understanding the fundamental properties of these materials at the atomic level and predicting their behavior in various applications. Such methods allow for a detailed analysis of interatomic interactions, charge and energy transfer between layers in heterostructures, as well as the influence of external factors (e.g., deformation, electric field). This facilitates a deeper understanding of the physical mechanisms underlying the observed electronic and optical phenomena. A clear comprehension of the fundamental electronic and optical processes in these heterostructures is critical for optimizing their performance and for the rational design of new functional devices. This is particularly relevant in the field of 1D and 2D materials, where a vast number of potential monolayer combinations exists. First-principles studies can significantly narrow the scope of experimental searches by identifying the most promising nanoheterostructures. For instance, first-principles calculations demonstrate that the band gap of 2D TMD heterostructurescan be modulated by an external electric field (Li *et al*. 2017). Such effects enable the control of excitonic states in TMD heterostructures using an electric field for promising applications in LEDs. The works (Jiang *et al*. 2021, Richter 2024) considered interlayer exciton relaxation processes, including population recombination dynamics, intervalley scattering processes, and polarized valley dynamics in 2D vdW TMD nanoheterostructures. In such nanostructures, interlayer exciton transfer is significantly enhanced due to both an external electric field and a moiré potential. It is worth noting that moiré effects also significantly influence the electronic and optical properties of vdW nanoheterostructures (Brem *et al*. 2020, Li *et al*. 2023, Sergeyev *et al*. 2023).

Another aspect of considerable interest isare first-principles calculations to search for new quantum transport properties of 1D and 2D nanoheterostructures (Sergeyev 2020b, Sergeyev *et al*. 2021a). In this work, using density functional theory, the electronic and optical properties of vdW nanotubes $WS_2(6,6)@MoS_2(14,14)$ and $WS_2(8,8)@MoS_2(16,16)$ the influence of an external electric field are modeled and analyzed.

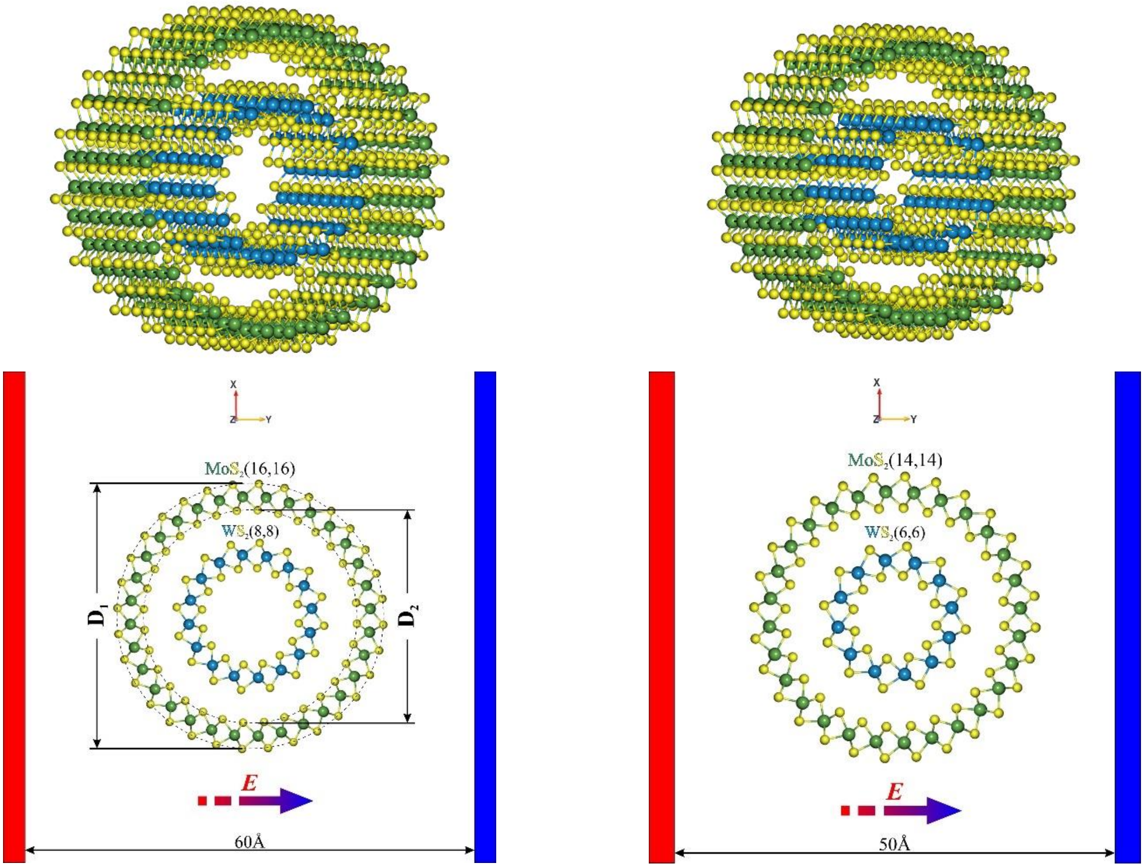

(a) (b)

Fig. 1 Geometry of one-dimensional Van der Waals nanostructures: a) WS$_2$(8,8)@MoS$_2$(16,16); b) WS$_2$(6,6)@MoS$_2$(14,14) (metallic electrodes are marked in red and blue)

Table 1 Geometric parameters of single-walled MoS$_2$(n,n) nanotubes

MoS$_2$(n,n)	D$_1$ (Å)	D$_2$ (Å)
(6,6)	8.807	14.981
(8,8)	12.128	18.438
(10,10)	15.549	21.928
(12,12)	19.028	25.444
(14,14)	22.522	28.965
(16,16)	26.048	32.509

Table 2 Geometric parameters of single-walled WS$_2$(n,n) nanotubes

WS$_2$(n,n)	D$_1$ (Å)	D$_2$ (Å)
(6,6)	8.668	14.756
(8,8)	11.918	18.146
(10,10)	15.287	21.582
(12,12)	18.68	25.024
(14,14)	22.137	28.506
(16,16)	25.59	31.98

2. Structure geometry

The geometric parameters of the optimized MoS$_2$(n,n) and WS$_2$(n,n) nanotubes (where n varies from 6 to 16) are given in Tables 1 and 2. The procedure for optimizing the geometry of the nanotubes and describing the interatomic interaction was performed with DFT, employing the generalized gradient approximation GGA-PBE (Bhattacharjee *et al*. 2024) as the exchange-correlation functional. The geometry optimization of the nanostructures was performed with threshold values of force and stress of 0.02 eV/Å and 0.001 eV/Å, respectively. For optimization, we used a grid with a cutoff energy of 360 Ry.

As can be seen from Tables 1 and 2, the most suitable nanotubes for coaxial connection by van der Waals forces to obtain nanoheterostructures are the following structures:

$$WS_2(8,8) + MoS_2(16,16) \rightarrow WS_2(8,8)@MoS_2(16,16);$$

$$WS_2(6,6) + MoS_2(14,14) \rightarrow WS_2(6,6)@MoS_2(14,14).$$

These nanotubes have the appropriate diameters for the intercalation of a small-sized tube (WS$_2$(n,n), n = 6, 8) into a larger diameter tube (MoS$_2$(n, n), n = 14, 16). For example, the outer diameter (D$_1$) of the WS$_2$(8,8) nanotube is 18.146 Å, and the inner diameter of the MoS$_2$(16,16) nanotube (D$_2$) is 26.048 Å, which allows creating a 1D vdW nanoheterostructure based on them. The geometry of the 1D vdW nanoheterostructures WS$_2$(6,6)@MoS$_2$(14,14), WS$_2$(8,8)@MoS$_2$(16,16) is shown in Fig. 1.

The considered vdW nanoheterostructures are placed (along the Y-axis) between metallic plates. To create an electric field, a positive potential (from 0 to 25 V) will be applied to the red electrode, while the blue electrode is neutral. Consequently, the electric field is directed from the red electrode to the blue electrode.

3. Basic equations

Computer modeling of the optimized nanotubes optical characteristicswas carried out within the framework of DFT-GGA using the Kubo-Greenwood equation, which defines their dielectric susceptibility (Khanjani *et al*. 2025, Sergeyev *et al*. 2021b):

$$\chi_{ij}\left(\omega\right)=-\frac{e^2\hbar^4}{m_e^2\varepsilon_0 V\omega^2}\sum_{nm}\frac{f\left(E_m\right)-f\left(E_n\right)}{E_{nm}-\hbar\omega-i\hbar\Gamma}\pi^i_{nm}\pi^j_{mn} \qquad (1)$$

where π^i_{nm} is *i*-component of the dipole matrix element between state *n* and *m*, *V* the volume, Γ the broadening, and $f(E)$ is the Fermi distribution function of quasiparticle energy, *e* is the charge of the electron, $\hbar$ is the Planck's constant, *E* is energy, ε_0 the vacuum permittivity, ω is the frequency and m_e is the mass of the electron.

From Eq. (1), the dependence of the dielectric permittivity on frequency (or energy) is determined:

$$\varepsilon\left(\omega\right)=1+\chi\left(\omega\right) \qquad (2)$$

Using the well-known Kramers-Kronig relation $\left(n+ik\right)^2=\left(\varepsilon'+i\varepsilon''\right)\mu$ (ε' is real part and ε'' is imaginary part of the complex dielectric permittivity, μ is the magnetic constant)), describing the relationship between the imaginary and real components of the complex dielectric permittivity (2) and optical quantities, we find the extinction coefficient k and the refractive index n of the nanotubes:

$$k\left(\omega\right)=\sqrt{\frac{\sqrt{\mathrm{Re}(\varepsilon)^2+\mathrm{Im}(\varepsilon)^2}-\mathrm{Re}(\varepsilon)}{2}} \qquad (3)$$

$$n\left(\omega\right)=\sqrt{\frac{\sqrt{\mathrm{Re}(\varepsilon)^2+\mathrm{Im}(\varepsilon)^2}+\mathrm{Re}(\varepsilon)}{2}} \qquad (4)$$

From Eq. (3), the optical absorption coefficient is determined:

$$\alpha=2\frac{\omega}{c}k \qquad (5)$$

When calculating the optical characteristics of the nanotubes, the expansion of the Kohn-Sham orbitals was carried out using an atomic orbital basis with double zeta polarization, while the wave functions of the electrons were expanded with a grid cutoff energy of 360 Ry. The k-points of the Brillouin zone, 1×1×30, were chosen using the Monkhorst-Pack package (Morgan *et al*. 2020). To calculate the real and imaginary parts of the dielectric function, an optical grid of 3×3×33 with a broadening of 0.1 was used.

To ensure the reliability of the obtained results, the following validation measures were implemented. First, the band gap of the MoS_2 monolayer during the 2D → 1D transition was evaluated and compared with available experimental data to confirm consistency. Second, selective verification of the computational results was performed by repeating the calculations using alternative software packages (Quantum ESPRESSO and BAND–Amsterdam Modeling Suite) to rule out errors associated with the implementation of the chosen method.

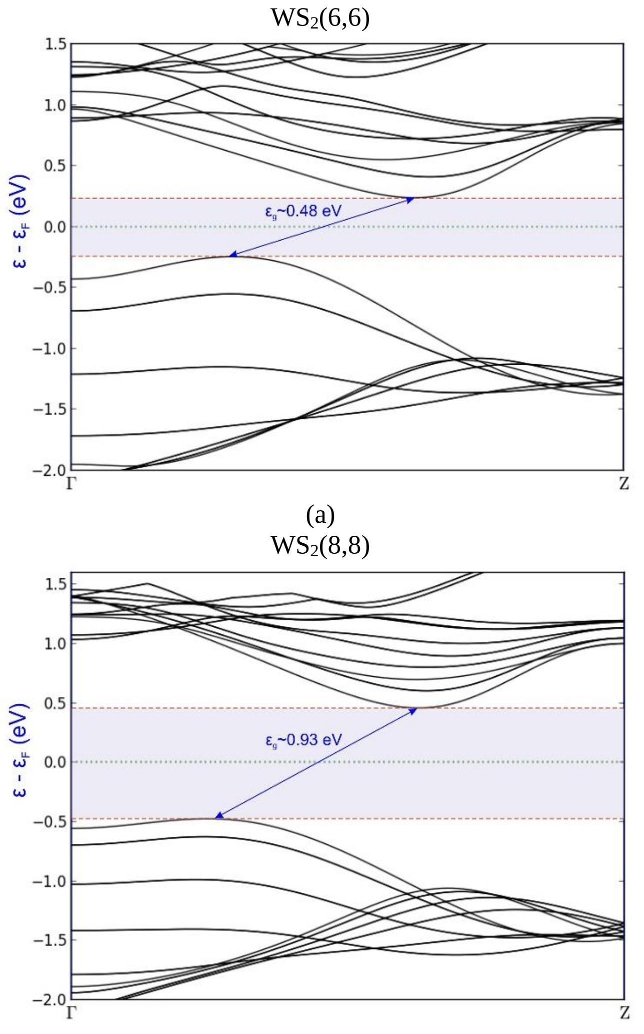

(a)

(b)

Fig. 2 Electronic band structure of $WS_2(6,6)$ and $WS_2(8,8)$ nanotubes

4. Results and discussion

We consider the properties of single-walled nanotubes $WS_2(6,6)$, $WS_2(8,8)$, $MoS_2(14,14)$, and $MoS_2(16,16)$, as components of the nanoheterostructures $WS_2(8,8)$@$MoS_2(16,16)$ and $WS_2(6,6)$@$MoS_2(14,14)$. The results of calculating their electronic band structure, calculated along the high symmetry point Γ-Z in the Brillouin zone, are shown in Figures 2 and 3. As can be seen, single-walled armchair $MoS_2(n,n)$ and $WS_2(n,n)$ nanotubes are semi-conductors with an indirect band gap. We recently showed that nanotubes with chirality (n, 0), i.e., $MoS_2(n,0)$ and

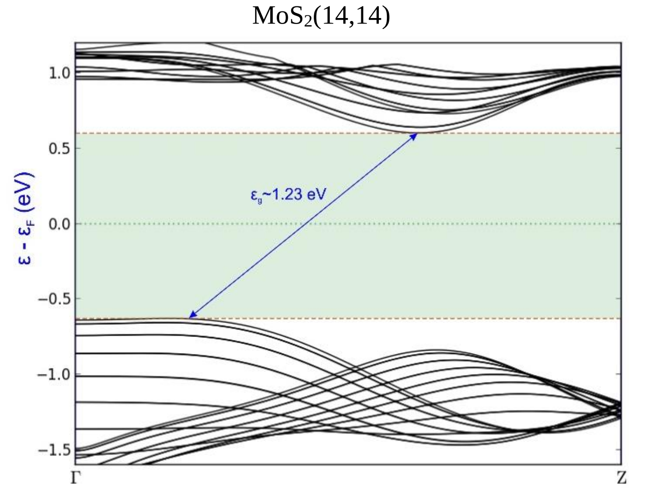

(a)

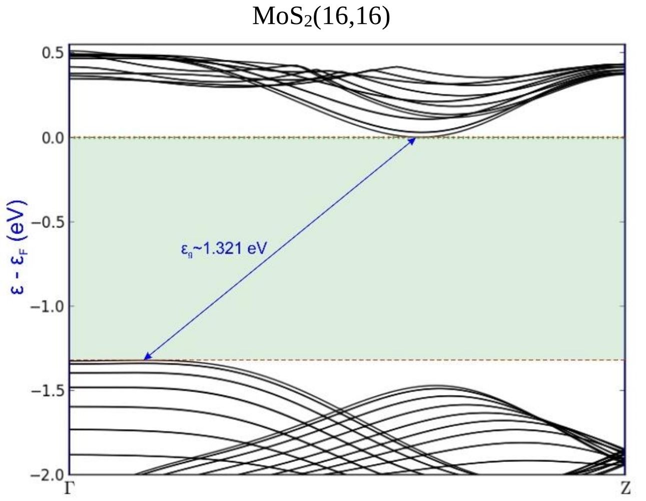

(b)

Fig. 3 Electronic band structure of $MoS_2(14,14)$ and $MoS_2(16,16)$ nanotubes

$MoSe_2(n,0)$, are semiconductors with a direct band gap at the Γ symmetry point (Sergeyev *et al*. 2024b).

With an elevation in the diameter of the nanotubes, an expansion in the band gap is observed. For example, $WS_2(6,6)$ has a gap of 0.48 eV, and $WS_2(8,8)$ has a gap of 0.93 eV (see Fig. 2). A similar pattern, the enlargement of the MoS_2 nanotube's band gap with a larger diameter, is also demonstrated in the work (Ansari *et al*. 2015), where the SIESTA program (DFT-GGA method) was used to calculate the electronic properties.The band gap results for the MoS_2 nanotubes in our work deviate slightly from the results of the previously mentioned work by Ansari, which we believe is due to the use of different programs for optimizing the geometry of the nanotubes, as well as for the implementation of the DFT-GGA method. For example, the band gap of $MoS_2(14,14)$ in the previously mentioned work is ~1.1 eV, while according to our calculations, it is ~1.2 eV.

We consider the optical properties of $WS_2(n,n)$ nanotubes (for n = 6, 8) and $MoS_2(n,n)$ nanotubes (for n = 14, 16) calculated parallel to the Z-axis. Fig. 4 shows the calculation results of the real and imaginary parts of the complex dielectric function of $MoS_2(n,n)$ and $WS_2(n,n)$ nanotubes. (Calculations of the real and imaginary parts of the complex dielectric function were performed based on equations (1-5)).

We note that in the energy range from 2.175 eV to 2.325 eV, the real part of the dielectric function Re(ε) of the $WS_2(6,6)$ nanotube becomes negative, having values from -0.11273 to -0.06088, with an extremum of -0.22514 at 2.25 eV. Accordingly, the value of the plasmon frequency ω_{pl} of the $WS_2(6,6)$ nanotubes varies from 526 THz to 562 THz.

The $MoS_2(10,10)$ nanotubes possess a high plasmon frequency ω_{pl} of 513.823÷519.868 THz. It is worth noting that the plasmon frequency values of both the $MoS_2(6,6)$ and $MoS_2(10,10)$ nanotubes lie in the visible region of the spectrum (Fig. 4a).

The values of the static dielectric permittivity ε_s for the $WS_2(n,n)$ and $MoS_2(n,n)$ nanotubes under consideration are presented in Table 1. (Note that here, static permittivity refers to the value of the dielectric permittivity at zero frequency, which is above interband transitions and below the frequency of phonons (Kumar *et al*. 2023)). As can be seen, the static dielectric permittivity decreases with increasing nanotube diameter. This is quite logical, since, according to the well-known Penn model (Lamichhane 2023), the value of the static dielectric permittivity is inversely proportional to the width of the bandgap $\left(\varepsilon \propto \frac{1}{\varepsilon_g}\right)$, and is described by the following approximate formula:

$$\varepsilon \approx 1+\left(\frac{\hbar\omega_p}{\varepsilon_g}\right) \tag{6}$$

where ω_p is the plasma frequency. In turn, the band gap width increases with increasing diameter of the TMD-nanotubes (Figs. 2, 3).

According to Eq. (3), derived from the Kramers-Kronig dispersion relation taking into account the properties of a non-magnetic medium, the extinction coefficient k and the optical absorption coefficient α are significantly dependent on the imaginary part of the dielectric permittivity Im(ε). Therefore, the main peaks of these functions, in most cases, appear at the same energy values (see, for example, Figs. 4b and 5a).

The results of calculating the absorption coefficient and refractive index of the considered single-wallednanotubes $WS_2(n,n)$ and $MoS_2(n,n)$ are shown in Figs. 5a-b. Fig. 5a depicts that the main absorption peaks of ~0.021 nm^{-1} and ~0.0853 nm^{-1} of the $WS_2(6,6)$ nanotube occur at energies of 2.17 eV and 2.975 eV, respectively, i.e. in the visible region of the spectrum (~570 nm,~416.75 nm).The main absorption bands of the $WS_2(8,8)$ nanotube, ~0.01 nm^{-1}, ~0.0115 nm^{-1}, and ~0.00356 nm^{-1}, appear at energies of 1.9 eV, 2.4 eV, and 3.025 eV, respectively. The $MoS_2(14,14)$ nanotube absorbs at 1.9 eV and 2.15 eV, while the $MoS_2(16,16)$ nanotube absorbs at 1.95 eV. As the diameter of the nanotubes increases, a decrease in absorption intensity is observed, as well as a shift of the absorption band towards a relatively higher energy region (Fig. 5a).

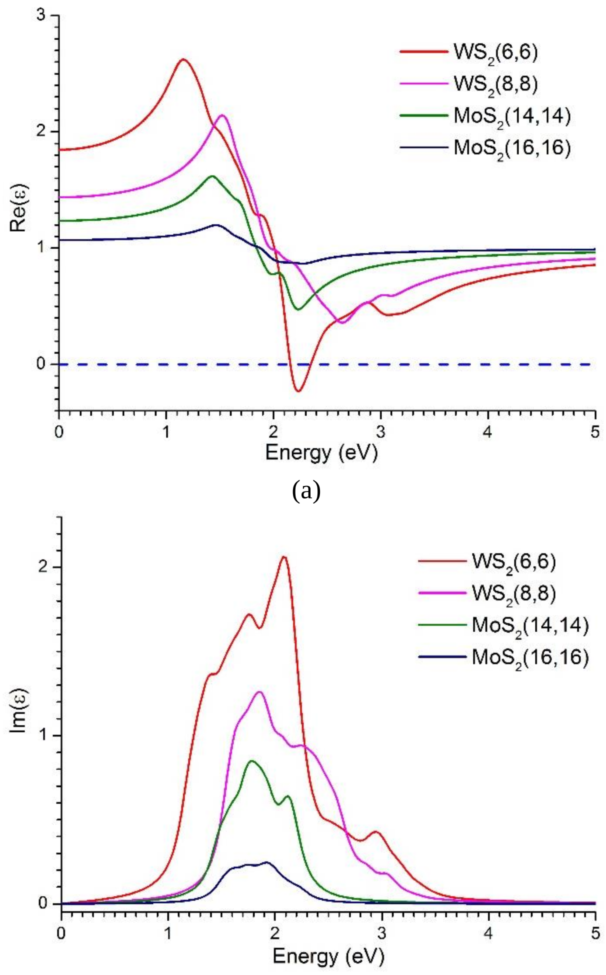

(a)

(b)

Fig. 4 Dependence of the complex dielectric permittivity of MoS_2(n,n) and WS_2(n,n) nanotubes: a) real part; b) imaginary part

For example, as shown above, the main maximum peak for WS_2(6,6) appears at 2.175 eV, while the main maximum peak for WS_2(8,8) appears at 2.4 eV. The same trend is observed in MoS_2 and $MoSe_2$ nanotubes (Sergeyev *et al*. 2024). We believe that this is related to the atoms in smaller diameter nanotubes being in a more stressed state compared to the atoms in larger diameter nanotubes. For example, the equilibrium total strain energy for MoS_2(6,6) nanotubes is ~-11 keV, and for MoS_2(14,14) nanotubes is ~-25 keV (Ansari *et al*. 2015).

The energy dependence of the refractive index for the WS_2(n,n) and MoS_2(n,n) nanotubes under consideration is shown in Figure 5b. The values of the static refractive index (at U = 0 V) are listed in Table 3. Evidently, the refractive index decreases with increasing nanotube diameter. It is evident that the refractive index n of a lossless material is usually described as the square root of the product of its dielectric permittivity ε and magnetic permeability μ:

$$n(\omega)=\sqrt{\varepsilon(\omega)\mu(\omega)} \tag{7}$$

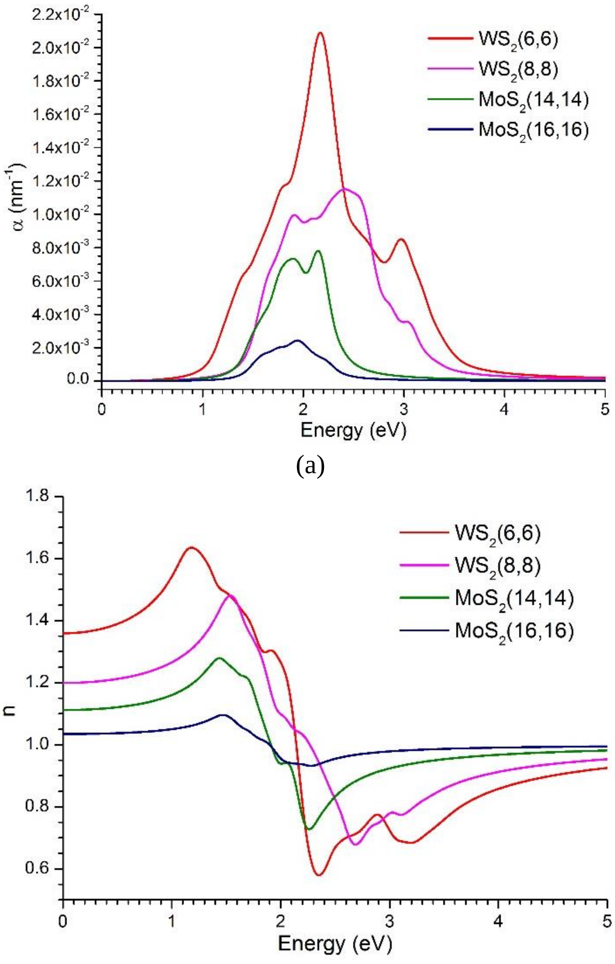

(a)

(b)

Fig. 5 Optical characteristics of MoS_2(n,n) and WS_2(n,n) nanotubes: a) absorption coefficient as a function of energy; b) refractive index as a function of energy

Table 3 Optoelectronic characteristics of single-walled WS_2 (n,n) and MoS_2(n,n) nanotubes at U = 0 V

	Band gap ε_g (eV)	Permittivity ε_s	Refractive index n
WS_2(6,6)	0.4837	1.84665	1.35892
WS_2(8,8)	0.93	1.43777	1.19907
MoS_2(14,14)	1.23	1.23611	1.11180
MoS_2(16,16)	1.321	1.0699	1.03436

Given that $\mu=1$ for non-magnetic media, we obtain $n(\omega)=\sqrt{\varepsilon(\omega)}$. Table 3 demonstrates that the static values of the refractive index are in very good agreement with this relationship. Near the absorption bands, the values of n deviate significantly from the static refractive index.

Now let's consider the properties of 1D nanodevices consisting of a combination of single-walled WS_2(n,n) and MoS_2(n,n) nanotubes connected by vdW interactions, the geometry of which is shown in Figure 1. The determined band structure results for the 1D devices WS_2(6,6)@MoS_2 (14,14) and WS_2(8,8)@MoS_2(16,16), calculated along the high-symmetry Γ-Z point in the Brillouin zone, are shown in Fig. 6.

We observe that the nanodevices, where WS_2 tubes of

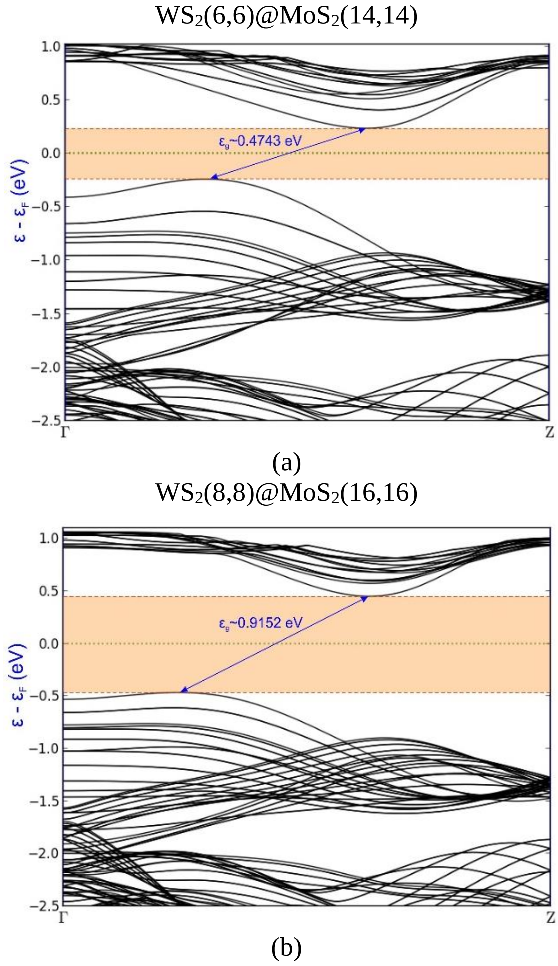

Fig. 6 Electronic band structure of 1D van der Waals nanoheterostructures: a) WS_2(6,6)@MoS_2(14,14); b) WS_2 (8,8)@MoS_2(16,16)

small radius are intercalated into MoS_2 tubes of large radius, exhibit a semiconducting nature. The bandgap widths of the semiconducting devices WS_2(6,6)@MoS_2 (14,14) and WS_2(8,8)@MoS_2(16,16) are 0.4743 eV and 0.9152 eV, respectively.

To investigate the chemical bonding underlying the ordering of nanostructures, the density of electronic states (DOS) associated with the constituent chemical elements is typically analyzed. For the considered 1D vdW heterostructures WS_2(6,6)@MoS_2(14,14) and WS_2(8,8)@MoS_2 (16,16), the partial contributions of the DOS from the s, p, and d orbitals of Mo, W, and S atoms are presented in Figs. 7 and 8, respectively. In the calculations, the widely used Grimme DFT-D3 correction was applied to account for London dispersion forces (van der Waals interactions), as long-range electron correlation effects are not adequately captured by standard DFT functionals. As shown, although the sulfur electrons are nominally located in the 3*s* and 3*p* orbitals, a minor contribution from sulfur *d*-electrons to the electronic structure is observed. Sulfur exhibits higher electronegativity compared to molybdenum and tungsten, which leads to a polarization of the electron density toward the sulfur atoms. While the primary valence electrons of sulfur occupy the 3*s* and 3*p* levels, the influence of neighboring Mo and W atoms can induce a small density of states in higher-lying *d* orbitals due to polarization effects. It is worth noting, however, that the *d*-orbital contribution of sulfur is negligible compared to that of Mo and W (see Figs. 7 and 8). The maximum DOS of sulfur *d*-electrons appears in the high-energy region and reaches only ~ 1.4 eV^{-1}, whereas the *d*-electron DOS values for Mo and W are

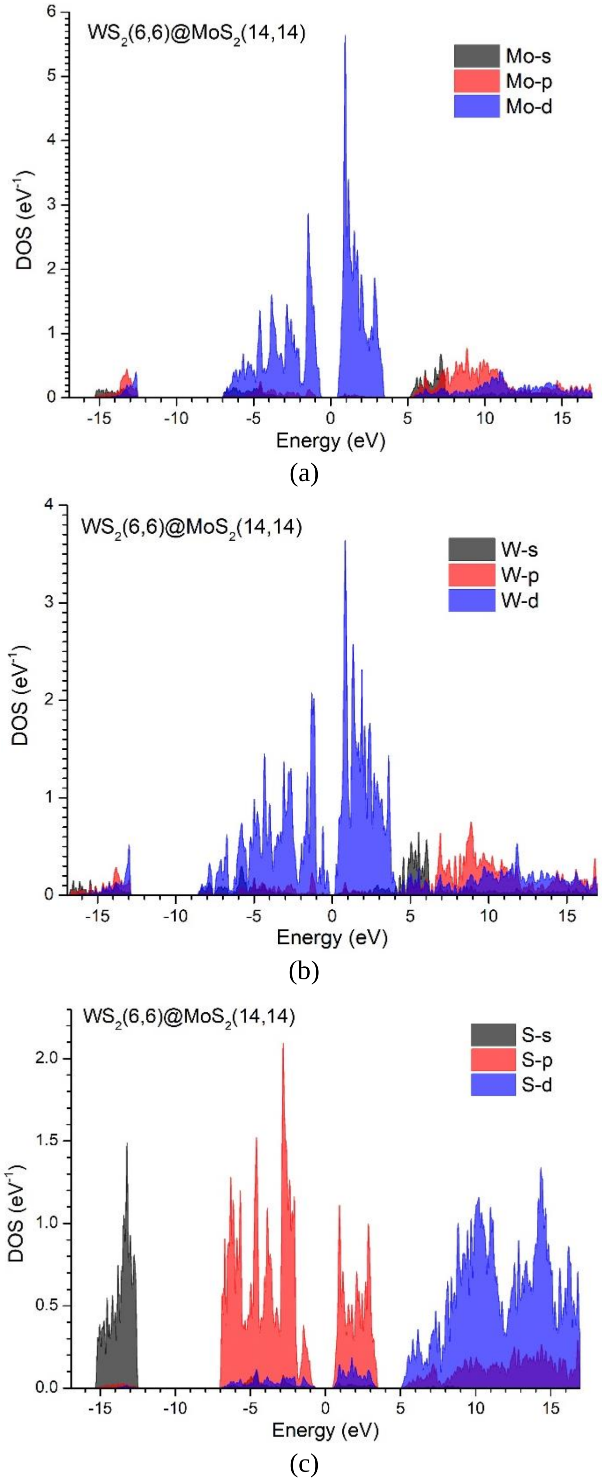

Fig. 7 Partial DOS contributions from the s, p, and d orbitals in DOS WS_2(6,6)@MoS_2(14,14) of the following elements: a) Mo; b) W; c) S

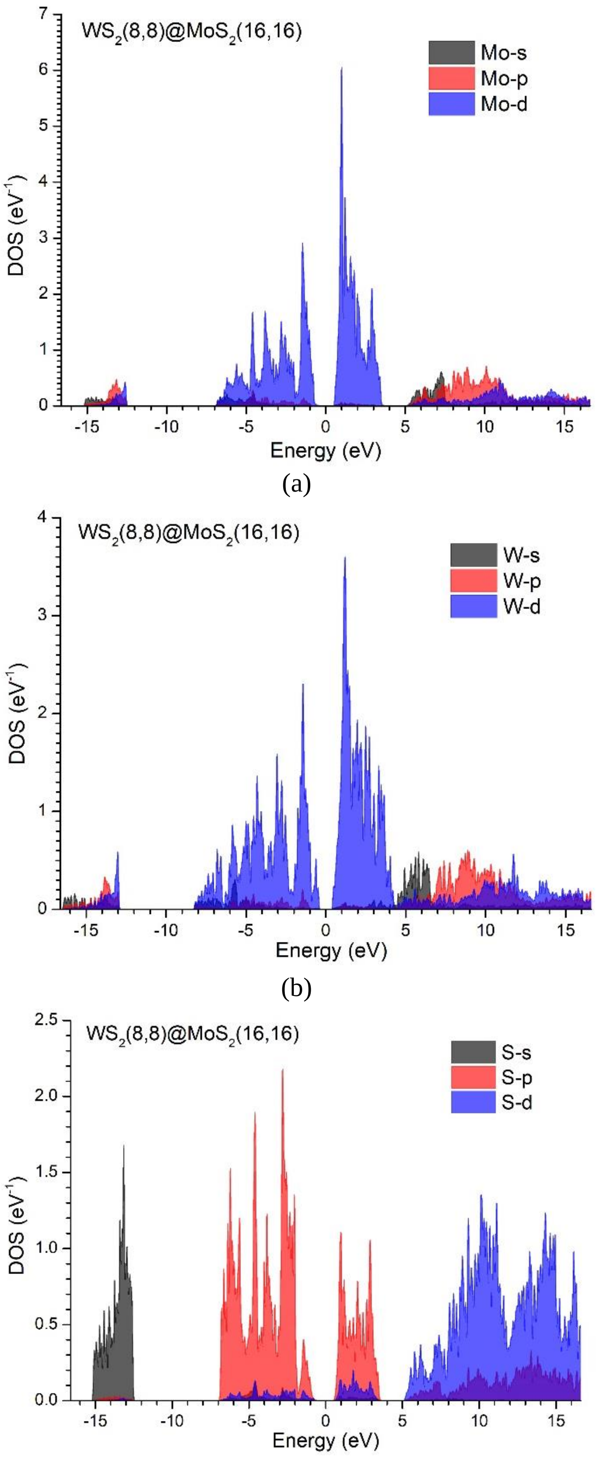

(a)

(b)

(c)

Fig. 8 Partial DOS contributions from the s, p, and d orbitals in DOS WS$_2$(8,8)@MoS$_2$(16,16) of the following elements: a) Mo; b) W; c) S

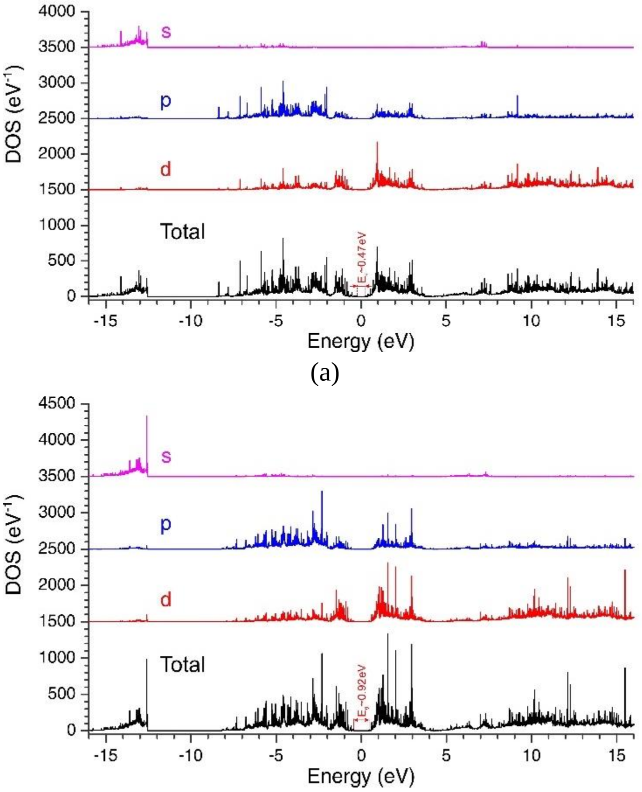

(a)

(b)

Fig. 9 Total DOS of the 1D vdW heterostructures: a) WS$_2$(6,6)@MoS$_2$(14,14); b) WS$_2$(8,8)@MoS$_2$(16,16). For clarity, the curves are vertically offset

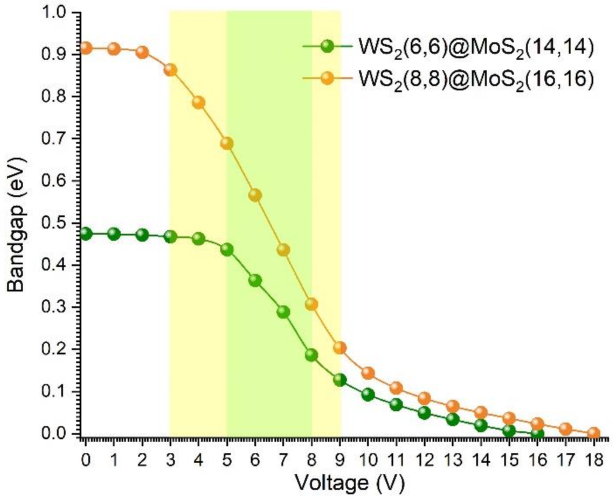

Fig. 10 Dependence of the band gap width of 1D nano-heterostructures on the applied voltage

approximately ~ 6 eV^{-1} и ~ 4 eV^{-1}, respectively. During the formation of Mo–S and W–S chemical bonds, atomic orbitals hybridize to form molecular orbitals. In this process, the 3*s* and 3*p* orbitals of sulfur may hybridize with the 4*d* and 5*s* orbitals of Mo, and the 5*d* and 6*s* orbitals of W. Higher *d* orbitals of sulfur may also contribute slightly to this hybridization, although their energies are significantly higher than those of the valence orbitals. In such electronic structures, which depend on intra-layer orbital hybridization in each TMD layer, electrons can fluctuate readily, forming temporary dipoles that affect dispersion forces and strengthen van der Waals interactions between the layers.

The total DOS of the examined nanostructures is presented in Fig. 9. As shown, for WS$_2$(6,6)@MoS$_2$(14,14),

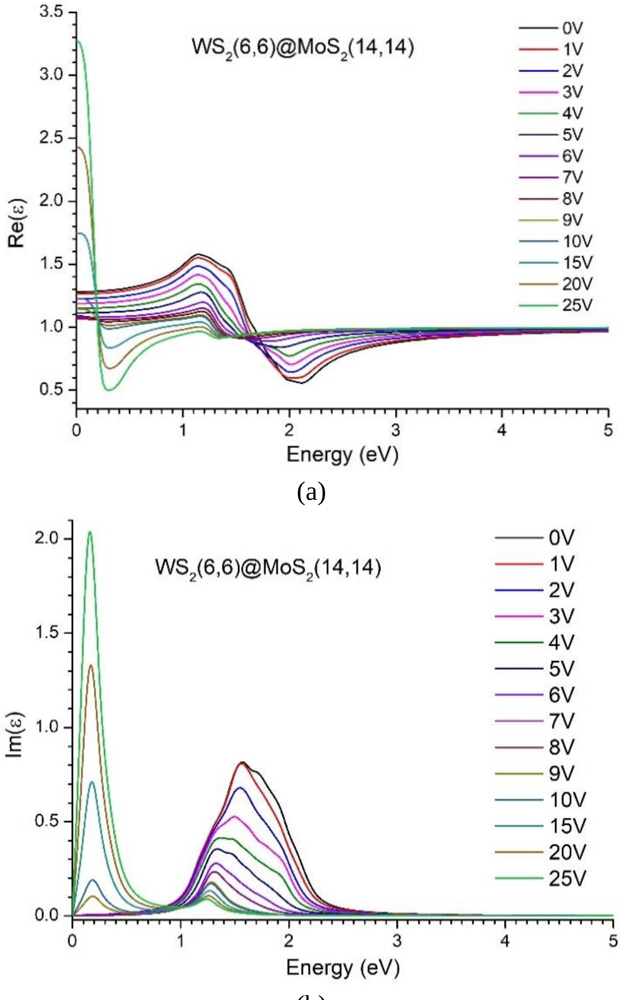

(a)

(b)

Fig. 11 Evolution of the complex dielectric function of the nanoheterostructure WS$_2$(6,6)@MoS$_2$(14,14) with an increase in voltage from 0 to 25 V: a) Re(ε); b) Im(ε)

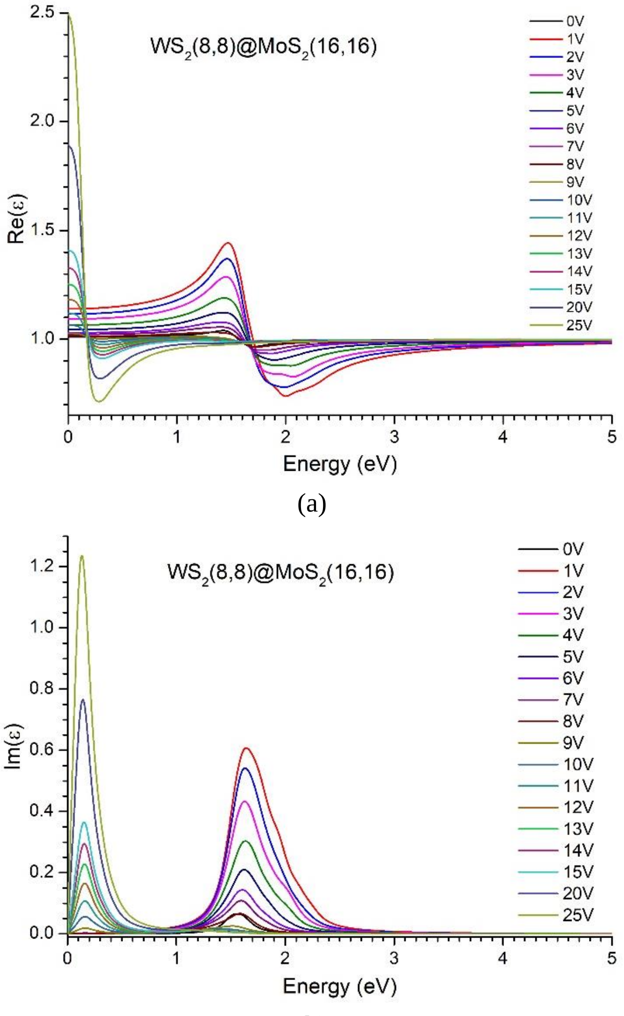

(a)

(b)

Fig. 12 Evolution of the complex dielectric function of the nanoheterostructure WS$_2$(8,8)@MoS$_2$(16,16) with an increase in voltage from 0 to 25 V: a) Re(ε); b) Im(ε)

no allowed electronic states are observed near the Fermi level in the range from –0.24 eV to 0.23 eV, resulting in a band gap of ~0.47 eV (Fig. 9a). Similarly, for WS$_2$(8,8)@MoS$_2$(16,16), the absence of states in the range from –0.463 eV to 0.457 eV indicates a band gap of ~0.92 eV (Fig. 9b). The band gap values derived from the DOS agree well with those obtained from the band structure analysis (see Fig. 6).

Fig. 10 shows the dependence of the bandgap width on the applied voltage for 1D nanoheterostructures WS$_2$(6,6)@MoS$_2$(14,14) and WS$_2$(8,8)@MoS$_2$(16,16). With an increase in the influence of the external electric field, the band gap width of the vdW nanoheterostructures decreases. In the voltage range from 3 V to 9 V, the band gap width of the WS$_2$(8,8)@MoS$_2$(16,16) nanoheterostructure decreases intensely according to a linear law (highlighted with a yellow background in the figure). A similar decrease in the bandgap width of WS$_2$(6,6)@MoS$_2$(14,14) occurs in the voltage range from 5 V to 8 V (highlighted with a green background in the figure). Above the specified voltages, the bandgap width of the nanoheterostructures decreases exponentially according to an exponential law: in the case of WS2(8,8)@MoS$_2$(16,16) – from 9 V to 18 V, and in the case of WS$_2$(6,6)@MoS$_2$(14,14) – from 8 V to 16 V. Upon reaching an external voltage of 16 V (and higher), the WS$_2$(6,6)@MoS$_2$(14,14) nanoheterostructure transitions from a semiconducting state to a metallic state. A similar transition occurs in the WS$_2$(8,8)@MoS$_2$(16,16) nanoheterostructures at a voltage of 18 V and higher (Fig. 10). Thus, the electric field can modulate the bandgap of the nanostructure, reducing its width, which allows the material to absorb photons with less energy. This expands the spectral absorption range and can increase the absorption coefficient in certain regions.

Figs. 11 and 12 show the evolution of the real and imaginary parts of the complex dielectric function of 1D nanoheterostructures WS$_2$(6,6)@MoS$_2$(14,14) and WS$_2$(8,8)@MoS$_2$(16,16) with an increase in external electric voltage from 0 to 25 V, respectively. (Note that in the presence of relaxation processes, the dielectric permittivity is considered in complex form). Consider the case where examine the dynamics of changes in the dielectric permittivity of the vdW nanodevice WS$_2$(6,6)@MoS$_2$ (14,14) at zero energy

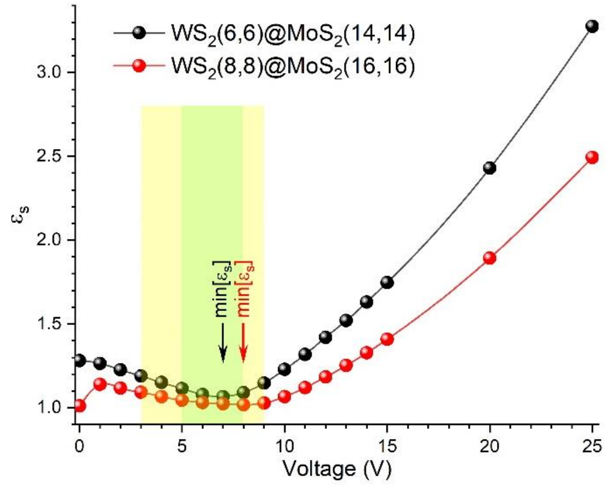

Fig. 13 Dependence of the static dielectric permittivity of 1D nanoheterostructures on the applied voltage

Table 4 Optical and electronic characteristics of 1D van der Waals nanostructures based on WS$_2$(n,n) and MoS$_2$(n,n) in the absence of an external electric field

1D nanoheterostructure	Band gap ε_g (eV)	Permittivity ε_s	Refractive index n
WS$_2$(6,6)@MoS$_2$(14,14)	0.4743	1.41962	1.191478
WS$_2$(8,8)@MoS$_2$(16,16)	0.9152	1.09609	1.046943

(Fig. 13). Under the influence of an external voltage from 0 V to 7 V, the value of the static dielectric permittivity decreases from 1.28121 to 1.06655, respectively. A further increase in voltage leads to a significant increase in the value of the static dielectric permittivity from 1.08996 to 3.27536. Typically, the smaller the band gap width, the higher the dielectric permittivity. In materials with a small ε_g, electrons are more easily excited into the conduction band, which will lead to an increase in electronic polarization. Note that the sharp linear decrease in the bandgap width is accompanied by a moderate change in the static dielectric permittivity (highlighted in yellow in Fig. 13).

Under the influence of an external electric field, we observe a similar behavior for the WS$_2$(8,8)@MoS$_2$(16,16) vdW nanodevice. A characteristic of (8,8)@MoS$_2$(16,16) relative to the previous one is the increase in ε_s from 1.01061 to 1.13997 in the voltage range of 0 to 1 V.

As can be seen from Figs. 11 and 12, a decrease in the real part of Re(ε) occurs near the maximum of the imaginary part of Im(ε). Note that such behavior of Re(ε) and Im(ε) as a function of energy is quite natural and is a specific example of the Kramers-Kronig dispersion relation (Rousseau *et al*. 2021). It is also noticeable that with an increase in the magnitude of the external electric field, the amplitude of the main peak of Im(ε) decreases and also shifts towards the lower energy region. For example, in the case of WS$_2$(6,6)@MoS$_2$(14,14), we observe a shift of the main peak from ~1.56 eV to ~1.23 eV. Moreover, the shift of the main peak is accompanied by the appearance of a second peak in Im(ε) (at ~1.6÷1.86 eV for the WS$_2$(6,6)@MoS$_2$(14,14) structure and at ~1.31÷1.62 eV for WS$_2$(8,8)@MoS$_2$(16,16)) and an increase in its amplitude.

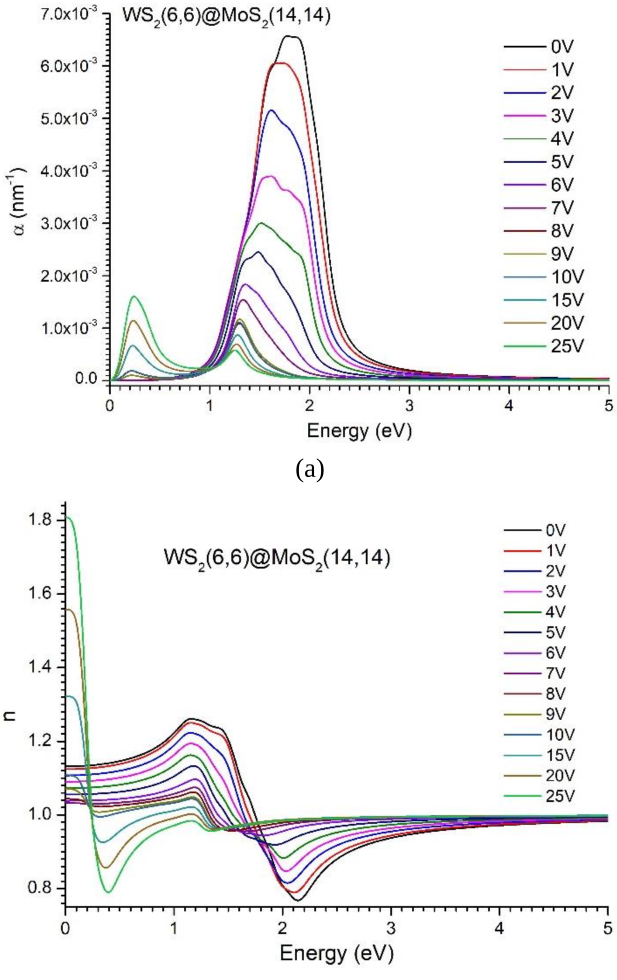

(a)

(b)

Fig. 14 Evolution of the absorption coefficient (a) and refractive index (b) of the WS$_2$(6,6)@MoS$_2$(14,14) nanostructure with increasing voltage from 0 to 25 V

Note that the dielectric permittivity is related to the polarizability of an atom according to the well-known Clausius-Mossotti formula (Eremin *et al*. 2021):

$$\frac{\varepsilon-1}{\varepsilon+2}=\frac{1}{3\varepsilon_0}\sum N_j a_j \tag{7}$$

where ε_0 is the electric constant, N_j is the number of atoms per unit volume exhibiting polarizability a_j. (Traditionally, atomic polarizability is denoted by the letter α; since in our case itis used to denote the absorption coefficient, we replaced it with a). Typically, in the optical frequency range, the dielectric permittivity is entirely attributed to electronic polarizability. Note that the band gap width primarily affects electronic polarization, as it determines the energy required to excite electrons. The features of the functions Im(ε) and Rm(ε) in the optical frequency range correspond to the electronic polarizability of the atoms of the structure under consideration, caused by the displacement of the electron shell of the atom relative to the

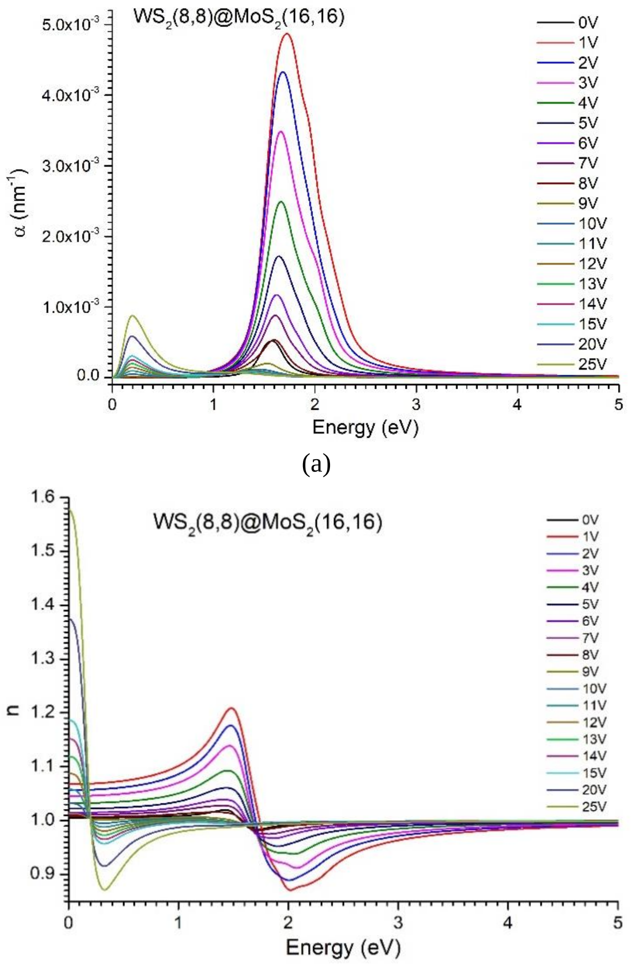

(a)

(b)

Fig. 15 Evolution of the absorption coefficient (a) and refractive index (b) of the WS$_2$(8,8)@MoS$_2$(16,16) nanostructure with increasing voltage from 0 to 25 V

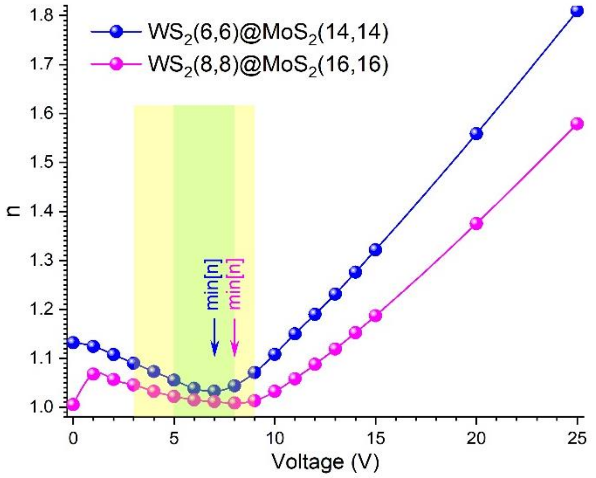

Fig. 16 Dependence of the static refractive index of 1D nanostructures on the applied voltage

nucleus. With an increase in the influence of the external electric field, we observe, in the nanoheterostructure, ionic polarizability caused by the displacement of charged ions relative to other ions. All the above-mentioned features of the complex dielectric function of 1D nanoheterostructures under the influence of an external electric field are explained by the presence of ionic polarizability, whose contribution increases with the field strength.

Subject to an external electric field, the values of the static dielectric permittivity ε_s of vdW nanohetero-structures WS$_2$(6,6)@MoS$_2$(14,14) and WS$_2$(8,8)@MoS$_2$(16,16) increase; for example, at a voltage of 25 V, the structures exhibit dielectric permittivities of 3.27536 and 2.49347, respectively. It is known that the static dielectric permittivity characterizes the ability of a material to polarize in a constant electric field. The increase in the value of ε_s occurs due to the redistribution of charges under the influence of an external electric field. (The main optoelectronic characteristics of 1D vdW nanohetero-structures based on WS$_2$(n,n) and MoS$_2$(n,n) in the absence of an external electric field are given in Table 4). Such properties of the considered nanoheterostructure scan be used to develop various nanoelectronic devices (e.g., nanowires, nano-contacts, nanocapacitors, etc.).

According to Eqs. (3, 5), the features of the imaginary part of the dielectric permittivity Im(ε) of vdW nano-structures characterize energy absorption and are reflected in their absorption coefficient (Figs. 14a, 15a). Meanwhile, according to equation (4), the features of the real part of the dielectric permittivity are reflected in their refractive indices (Figs. 14b, 15b)

When the system is not subjected to an external electric field, the main absorption coefficient peaks of the WS$_2$(6,6) @MoS$_2$(14,14) structure, roughly ~$6.5\cdot10^{-3}$ nm^{-1}, are observed at energies of 1.8 eV and 1.9 eV. As the external electric field gradually increases, a decrease in the amplitude of the main absorption coefficient peaks is observed, concurrent with their shift from the high-energy region to the low-energy region (Figure 14a). At 9 V, only a single absorption peak remains at 1.3 eV, while a new absorption peak emergesat near ~0.22 eV. With further voltage increase, the contributionof the "high-energy" absorption component diminishes, while the "low-energy" component becomes more pronounced (Fig. 14a). This behavior of the absorption coefficient attributedto charge redistribution and an increase in the contribution of ionic polarizability in the nanostructure.

The absorption coefficient behavior of the WS$_2$(8,8) @MoS$_2$(16,16) nanostructure slightly differs from the previous structure (see Fig. 15a). Without an external electric field, the absorption coefficient peak of this structure, around~$5\cdot10^{-3}$nm^{-1}, appears at 1.6 eV. When a voltage of 1 V is applied, the absorption coefficient sharply increases to ~$5.8\cdot10^{-3}$ nm^{-1}. Further voltage increase up to 8 V leads to its reduction almost to the initial level, along with the appearance of a new peak at 0.2 eV. We assume that this behavior of the nanosystem is associated with the reconfiguration of atomic electronic polarizability. A further increase in external voltage from 9 V to 25 V enhances the contribution of ionic polarizability, accompanied by distinct peaks at 0.2 eV. Additionally, it is noteworthy that the emergence of a new peak in both considered nanostructures, WS$_2$(6,6)@MoS$_2$(14,14) and WS$_2$(8,8)@

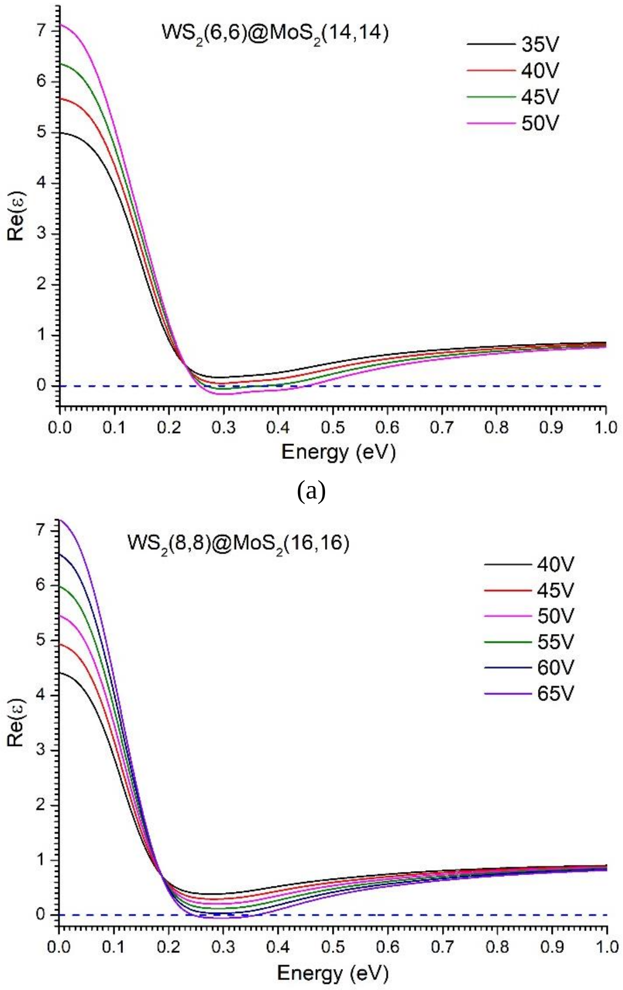

(a)

(b)

Fig. 17. Appearance of a negative value of Re(ε) with increasing external electric field: a) WS$_2$(6,6)@MoS$_2$ (14,14); b) WS$_2$(8,8)@MoS$_2$(16,16)

MoS$_2$(16,16), corresponds to voltage values of 8 V and 9 V, respectively, where the sharp linear decrease in bandgap width ends, transitioning to an exponential law of change (see Fig. 10).

In the considered vdW nanostructures of WS$_2$(6,6)@ MoS$_2$(14,14) and WS$_2$(8,8)@MoS$_2$(16,16), the refraction of electromagnetic radiation occurs over a relatively wide energy range (see Figs. 14b, 15b). Under the influence of an external electric field, the refractive index of the WS$_2$(6,6) @MoS$_2$(14,14) structure gradually decreases across the entire energy range in the voltage interval of 1÷7 V. Further voltage increase from 8 V and above leads to a dynamic change in the refractive index within the ~0÷0.8 eV range. A similar effect is observed in the WS$_2$(8,8)@ MoS$_2$(16,16) structure; however, in this case, the refractive index sharply increases at 1 V, followed by a gradual decrease as the voltage rises to 9 V (see Fig. 15b). As mentioned earlier, this behavior may be attributed to an electric field-induced charge redistribution in the nano-structure's energy bands. Notably, the dynamic variation of the refractive index in the low-energy region corresponds to voltages of 9 V and 8 V, respectively, where the sharp linear decrease in the bandgap width ends, transitioning to an exponential law of change (see Figs. 10, 15).

The dynamics of the static refractive index of vdW nanostructures as a function of the applied voltage is presented in Fig. 16. (The values of the static refractive index of vdW nanostructures in the absence of an external electric field are provided in Table 4). As seen, the static refractive index values align well with the classical equation (6), which defines the relationship between εs and n. The refractive indices of the nanostructures change slowly as the bandgap width decreases linearly (see Fig. 10). These properties of the considered nanostructures can be utilized in the development of nanodevices similar to a Luneburg lens, where the refractive index varies according to a specific law depending on the distance from the axis in cylindrical lenses (Mikhailikova *et al*. 2024).

Our calculations confirmed that, in the range of 2.175÷2.325 eV, WS$_2$ (6,6) nanotubes have a negative real part of the dielectric permittivity Re(ε) (see Fig. 4a). By enhancing the influence of the external electric field on vdW TMD-heterostructures, it is possible to achieve a negative value for the real part of the dielectric permittivity Re(ε) < 0. Such a condition (Re(ε) < 0) for the structure WS$_2$(6,6)@MoS$_2$(14,14) is fulfilled at 45 V and higher, while for WS$_2$(8,8)@MoS$_2$(16,16) it is achieved at 65 V and higher. Remarkably,in the interval 0.275–0.35 eV, the real part of the dielectric permittivity of WS$_2$(6,6)@MoS$_2$ (14,14) at 45 V ranges from -0.04348 to -0.01075 (with a minimum of -0.06276 at 0.3 eV) (see Fig. 17a). In the range 0.25–0.35 eV,the real part of the dielectric permittivity for the structure WS$_2$(8,8)@MoS$_2$(16,16) at 65V changes from -0.02777 to -0.01974 (with an extremum of -0.05528 at 0.3 eV) (see Fig. 17b). At negative values of Re(ε), the material does not support the propagation of electromagnetic waves in the classical sense. However, it is known that nanomaterials with a negative real part of the dielectric permittivity find applications in various fields of science and technology due to their unique interactions with electromagnetic waves. Such nanomaterials can be used in plasmonics and nanophotonics (Wang *et al*. 2024) for the creation of new types of nanoantennas, biosensors, plasmonic waveguides, and other nano-devices.

5. Conclusions

Thus, within the framework of the density functional theory (GGA-PBE), this study examinesthe electronic and optical properties of vdW nanostructures WS$_2$(6,6)@MoS$_2$ (14,14) and WS$_2$(8,8)@MoS$_2$(16,16), consideringthe influence of the external electric field. It has been demonstrated that with increasing external electric field strength, the band gap of the vdW nanostructures WS$_2$(6,6)@MoS$_2$(14,14) and WS$_2$(8,8)@MoS$_2$(16,16) decreases, and a transition from semiconducting to metallic behavior occurs at 16 V and 18 V, respectively. The evolution of the complex dielectric function of the 1D nanostructures WS$_2$(6,6)@MoS$_2$(14,14) and WS$_2$(8,8)@MoS$_2$(16,16) under increasing external electric field was analyzed, revealing that their static dielectric permittivity increases due to charge redistribution. It was shown that this redistribution of charge, along with an increase in the ionic polarizability within the nanostructures, leads to a decrease in the amplitude of the main absorption peaks and their shift from the high-energy region toward the low-energy region. Modulation of the dielectric response of the nanostructures by the external electric field was observed, which is attributed to both electronic and ionic polarization mechanisms. The studied nanomaterials show potential for use in adaptive optical systems and advanced nanoelectronic device components.

Acknowledgments

This research has is funded by the Science Committee of the Ministry of Science and Higher Education of the Republic of Kazakhstan (Grant No AP23488734)

References

Akhter, P., Ali, F., Ali, A. and Hussain, M. (2024), “TiO_2 decorated CNTs nanocomposite for efficient photocatalytic degradation of methylene blue”, *Diam. Relat. Mater.*, **141**, 110702. https://doi.org/10.1016/j.diamond.2023.110702

Ansari, R., Malakpour, S., Faghihnasiri, M. and Sahmani, S. (2015), “An ab initio investigation into the elastic, structural and electronic properties of MoS2 nanotubes”, *Superlatt. Microst.*, **82**, 188–200. https://doi.org/10.1016/j.spmi.2015.02.025

Arnaud, C., Lecouturier, F., Mesguich, D., Ferreira, N., Chevallier, G., Estournès, C., Weibel, A. and Laurent, C. (2016), “High strength – High conductivity double-walled carbon nanotube – Copper composite wires”, *Carbon*, **96**, 212-215. https://doi.org/10.1016/j.carbon.2015.09.061

Baithi, M. and Duong, D.L. (2024), “Doped, two-dimensional, semiconducting transition metal dichalcogenides in low-concentration regime”, *Crystals*, **14**, 832. https://doi.org/10.3390/cryst14100832

Bazbouz, M.B., Aziz, A., Copic, D., De Volder, M. and Welland, M.E. (2021), “Fabrication of high specific electrical conductivity and high ampacity carbon nanotube/copper composite wires”, *Adv. Electr. Mater.*, **7**, 2001213. https://doi.org/10.1002/aelm.202001213

Bhattacharjee, S., Koshi, N.A. and Lee, S.C. (2024), “Customizing PBE exchange-correlation functionals: a comprehensive approach for band gap prediction in diverse semiconductors”, *Phys. Chem. Chem. Phys.*, **26**(41), 26443-26452. https://doi.org/10.1039/d4cp03260h

Brem, S., Lin, K.Q., Gillen, R., Bauer, J.M., Maultzsch, J., Lupton, J.M. and Malic, E. (2020), “Hybridized intervalley moire excitons and flat bands in twisted WSe2 bilayers”, *Nanoscale*, **12**, 11088-11094. https://doi.org/10.1039/d0nr02160a

Cambre, S., Liu, M., Levshov, D., Otsuka, K., Maruyama, S. and Xiang, R. (2021) “Nanotube-based 1D heterostructures coupled by van der waals forces”, *Small*, **17**(38), 2102585. https://doi.org/10.1002/smll.202102585

Chaudhary, S.K. and Singh, K.K. (2021) “Complex phenomenal growth of multi-walled carbon nanotubes in conventional arc discharge process”, *T. Indian I. Metals*, **74**(8), 2043-2048. https://doi.org/10.1007/s12666-021-02316-4

Dhanasekaran, G., Parthiban, N., Keerthana, T., Gopal, R, Sangaraju, S., Chakrabortty, S. and Thangavel, E. (2025), “Enhanced electrochemical performance of (MoSe2@NiSe2) (0D/1D) hybrid nanostructures for supercapacitors”, *Mater. Sci. Eng. B Adv.*, **313**, 117975. https://doi.org/10.1016/j.mseb.2024.117975

Ding, D.D., Qu, Z.Z., Han, X.Y., Han, C.R., Zhuang, Q., Yu, X.L., Niu, R.R., Wang, Z.Y., Li, Z.X., Gan, Z.Z., Wu, J.S. and Lu, J.M. (2022), “Multivalley superconductivity in monolayer transition metal dichalcogenides”, *Nano Lett.*, **22**, 7919-7926. https://doi.org/10.1021/acs.nanolett.2c02947

Eremin, I.E., Neshchimenko, V.V., Shcherban, D.S. and Fomin, D.V. (2021), “System modification of the equation Lorenz–Lorentz–Clausius–Mossotti”, *Optik*, **231**, 166327. https://doi.org/ 10.1016/j.ijleo.2021.166327

Feng, Y., Li, H.N., Inoue, T., Chiashi, S., Rotkin, S., Xiang, R. and Maruyama, S. (2021), “One-Dimensional van der Waals Heterojunction Diode”, *ACS Nano*, **15**(3), 5600-5609. https://doi.org/10.1021/acsnano.1c00657

Guo, J., Xiang, R., Cheng, T., Maruyama, S. and Li, Y. (2022), “One-Dimensional van der Waals Heterostructures: A Perspective”, *ACS Nanosci.*, **2**, 3-11. https://doi.org/10.1021/acsnanoscienceau.1c00023

Guo, J., Zhai, L.X., Zhang, X.R., Sheng, J., Qiao, R.X., Liu, K.H., Xu, Z.P. and Li, Y. (2025), “Preparation of Single-Crystal MoS2 Nanotubes and 1D Van der Waals Heterostructures”, *Adv. Funct. Mater.*, **35**, 2408703. https://doi.org/10.1002/adfm.202408703

Guo, X.B., Yang, Z.T., Wang, W., Zhang, Y., Yu, N.F. and Lu, C.H. (2024), “Silicon/carbon nanotubes anode for lithium-ion batteries: Synthesis, interface and electrochemical performance”, *Surf. Interf.*, **48**, 104223. https://doi.org/10.1016/j.surfin.2024.104223

Hatakeyama, R., Ueno, H., Kwon, E. and Misaizu, F. (2024), “Critical plasma-processing-enabled growth of chirality-predefined single-walled carbon nanotubes from carbon nanorings”, *Appl. Phys. Express*, **17**(9), 096003. https://doi.org/10.35848/1882-0786/ad74d8

Jiang, Y., Chen, S.L., Zheng, W.H., Zheng, B.Y. and Pan, A.L. (2021), “Interlayer exciton formation, relaxation, and transport in TMD van der Waals heterostructures”, *Light Sci. Appl.*, **10**, 72. https://doi.org/10.1038/s41377-021-00500-1

Jin, C., Wu, Q.B., Yang, G.Q., Zhang, H.Y. and Zhong, Y.F. (2021), “Investigation on hybrid nanofluids based on carbon nanotubes filled with metal nanoparticles: Stability, thermal conductivity, and viscosity”, *Powder Technol.*, **389**, 1-10. https://doi.org/10.1016/j.powtec.2021.05.007

Jayakumari, B.Y., Swaminathan, E.N. and Partheeban, P. (2024), “Sustainable construction material using nanosilica and multi-walled carbon nanotubes in cement concrete”, *Adv. Nano Res.*, **16**(5), 459-472. https://doi.org/10.12989/anr.2024.16.5.459

Khanjani, S., Mohammadi-Manesh, E. and Ahmadvand, N. (2025), “Impact of metal doping on the electrical and optical properties of AgI2 QDs: A DFT study”, *Mat. Sci. Semicon. Proc.*, **194**, 109584. https://doi.org/10.1016/j.mssp.2025.109584

Kharlamova M.V. (2023), “Filled carbon nanotubes: Promising material for applications”, *Nanomaterials*, **13**(17), 2472. https://doi.org/10.3390/nano13172472

Kharlamova, M.V. and Kramberger, C. (2023), “Metal and metal halogenide-filled single-walled carbon nanotubes: Kinetics, electronic properties, engineering the fermi level”, *Nanomaterials*, **13**(1), 180. https://doi.org/10.3390/nano13010180

Kharlamova, M.V. and Kramberger, C. (2022), “Spectroscopy of filled single-walled carbon nanotubes”, *Nanomaterials*, **12**(1), 42. https://doi.org/10.3390/nano12010042

Kim, H., Johns, J.E. and Yoo, Y. (2020), “Mixed-Dimensional In-Plane Heterostructures from 1D Mo6Te6 and 2D MoTe2 ynthesized by Te-Flux-Controlled Chemical Vapor Deposition”, *Small*, **16**(47), 2002849. https://doi.org/10.1002/smll.202002849

Kumar, M.C. and Benazir, J.A. (2024), “Numerical and statistical analysis of Newtonian/non-Newtonian traits of MoS2-C2H6O2 nanofluids with variable fluid properties”, *Adv. Nano Res.*, **16**(4), 341-352. https://doi.org/10.12989/anr.2024.16.4.341

Kumar, K., Kumar, M. and Sharma, M. (2023), “Electronic and optical properties of α-TeX2 (X = S, Se) nanotubes: A first principle study", *Mater. Today Proc.*, In press. https://doi.org/10.1016/j.matpr.2023.01.255

Lamichhane, A. (2023), "Absorption in narrow and wide gap materials", *Heliyon*, **9**(11), e21507. https://doi.org/10.1016/j.heliyon.2023.e21507

Li, W., Wang, T.X., Dai, X.Q., Wang, X.L., Zhai, C.Y., Ma, Y.Q., Chang, S.S. and Tang, Y.A. (2017), "Electric field modulation of the band structure in MoS2/WS2 van der waals heterostructure", *Solid State Commun.*, **250**, 9-13. https://doi.org/10.1016/j.ssc.2016.11.006

Li, Y.H., Hao, S.L., Xu, N.N., Gao, Y., Qin, X.F., Chi, X.Y., He, N. and He, M.S. (2024), "Chirality-selective growth of single-walled carbon nanotubes from layered double hydroxide supported monometallic catalysts", *Chinese Sci. Bull.*, **69**(16), 2288-2297. https://doi.org/10.1360/TB-2023-0823

Li, X., Yuan, P., He, M., Li, L., Du, J., Xiong, W., Xia, C. and Kou, L. (2023), "Optoelectronic properties and applications of two-dimensional layered semiconductor van der Waals hetero-structures: perspective from theory", *J. Phys. Condens. Matter.*, **35**, 043001. https://doi.org/10.1088/1361-648X/aca5db

Liang, H.X., Wang, B.S., Su, R.H., Zhang, A., Wang, F.Q. and Shuai, Y. (2022), "Enhance photoelectric efficiency of PV by optical-thermal management of nanofilm reflector", *Adv. Nano Res.*, **13**(5) 475–485. https://doi.org/10.12989/anr.2022.13.5.475

Liu, M., Hisama, K., Zheng, Y., Maruyama, M., Seo, S., Anisimov, A., Inoue, T., Kauppinen, E.I., Okada, S. and Chiashi, S. (2021), "Photoluminescence from single-walled MoS2 nanotubes coaxially grown on boron nitride nanotubes", *ACS Nano*, **15**, 8418-8426. https://doi.org/10.1021/acsnano.0c10586

Matsushita, S., Otsuka, K., Sugihara, T., Zhu, G.Y., Kittipaisalsilpa, K., Lee, M., Xiang, R., Chiashi, S. and Maruyama, S. (2023), "Horizontal arrays of one-dimensional van der waals hetero-structures as transistor channels", *ACS Appl. Mater. Interf.*, **15**, 10965-10973. https://doi.org/10.1021/acsami.2c22964

Mikhailikova, I.O., Natarov, D.M., Dukhopelnykov, S.V., Sauleau, R., Lucido, M. and Nosych, O.I. (2024), "Tunable enhancement of the cylindrical Luneburg lens focusing ability with the aid of a conformal graphene strip", *Opt. Express*, **32**(23), 41726-41740. https://doi.org/ 10.1364/OE.529269

Mohammed, A.J., Mohammed, B.A., Kadhom, H.K., Taki, A.G. and Tahouneh, V. (2024), "A semi-analytical study for vibration analysis of damaged core laminated cylindrical shell with functionally graded CNTs reinforced face sheets resting on a two-parameter elastic foundation", *Adv. Nano Res.*, **17**(4), 301-313. https://doi.org/10.12989/anr.2024.17.4.301

Morgan, W.S., Christensen, J.E., Hamilton, P.K., Jorgensen, J.J., Campbell, B.J., Hart, G.L.W. and Forcade, R.W. (2020), "Generalized regular k-point grid generation on the fly", *Compos. Mater. Sci.*, **173**, 109340. https://doi.org/10.1016/j.commatsci.2019.109340

Moon, B.H. (2021), "Metal-insulator transition in two-dimensional transition metal dichalcogenides", *Emergent Mater.*, **4**, 989-998. https://doi.org/10.1007/s42247-021-00202-9

Qiu, Y., Yang, H.B., Wen, B., Ma, L. and Lin, Y. (2021), "Facile synthesis of nickel/carbon nanotubes hybrid derived from metal organic framework as a lightweight, strong and efficient microwave absorber", *J. Colloid Interf. Sci.*, **590**, 561-570. https://doi.org/10.1016/j.jcis.2021.02.003

Park, D., Kim, M. and Kim, J. (2023), "Coaxial structured Bi_2S_3-SnS_2-MWCNT hybrid nanocomposite with its improved thermoelectric properties", *Ceram. Int.*, **49**, 24904-24910. https://doi.org/10.1016/j.ceramint.2023.05.019

Poudel, Y.R., Zhao, X., Jungjohann, K.L., Thapa, A., Guo, R. and Li, W.Z. (2023), "Ni_3S_2 nanowires filled carbon nanotubes of ultra-high quality: Synthesis methods, structure, and electrical properties", *Diam. Relat. Mater.*, **127**, 109156. https://doi.org/10.1016/j.diamond.2022.109156

Rasulov, V.R., Rasulov, R.Y., Nasirov, M.K., Muminov, I.A. and Mamatova, M.M. (2024), "Theory of size quantization in monolayers of transition metal dichalcogenides", *Phys. Scr.*, **99** 105987. https://doi.org/10.1088/1402-4896/ad7546

Richter, M. (2024), "Theory of interlayer exciton dynamics in two-dimensional transition metal dichalcogenide heterolayers under the influence of strain reconstruction and disorder", *Phys. Rev. B*, **109**, 125308. https://doi.org/10.1103/PhysRevB.109.125308

Rousseau, E., Izard, N., Bantignies, J.L. and Felbacq, D. (2021), "Comment on the paper "Improving Poor Man's Kramers-Kronig analysis and Kramers-Kronig constrained variational analysis", *Spectrochim. Acta A*, **259**, 119849. https://doi.org/10.1016/j.saa.2021.119849

Sergeyev, D. (2021), "One-dimensional Schottky nanodiode based on telescoping polyprismanes", *Adv. Nano Res.*, **10**(4), 339-347. https://doi.org/10.12989/anr.2021.10.4.339

Sergeyev, D. (2020a), "Single electron transistor based on endohedral metallofullerenes Me@C_{60} (Me = Li, Na, K)", *J. Nano Electron. Phys.*, **12**(3), 03017. https://doi.org/10.21272/jnep.12(3).03017

Sergeyev, D. (2020b), "Features of the electrical characteristics of an octagraphene nanotube", *J. Nano Electr. Phys.*, **11**(6), 06022. https://doi.org/10.21272/jnep.11(6).06022

Sergeyev, D., Ashikov N. and Zhanturina N. (2021a), "Electric transport properties of a model nanojunction graphene–fullerene C60–Graphene", *Int. J. Nanosci.*, **20**(1), 2150007. https://doi.org/10.1142/S0219581X21500071

Sergeyev, D.M. and Duisenova, A.G. (2021), "Electron transport in model quasi-two-dimensional van der Waals nanodevices", *Tech. Phys. Lett.*, **47**(4), 375–378. https://doi.org/10.1134/S1063785021040295

Sergeyev, D., Duisenova, A. and Shunkeyev, K. (2024b), "Electronic and optical properties of one-dimensional Van Der Waals nanodevices based on MoS2(n,n) and MoSe2(n,n) nanotubes", *Crystals*, **14**(12), 1055. https://doi.org/10.3390/cryst14121055

Sergeyev, D., Duisenova, A., Solovjov, A. and Ismayilova, N. (2023), "Electron transport in a stressed moiré bigraphene structure", *Results Phys.*, **54**, 107140. https://doi.org/10.1016/j.rinp.2023.107140

Sergeyev, D., Shunkeyev K. and Solovjov A.L. (2024a), "On a model of a Josephson junction with a single quantum channel featuring a "deformed" Andreev reflection coefficient", *Low Temp. Phys.*, **50**, 976-981. https://doi.org/10.1063/10.0030414

Sergeyev, D., Zhanturina, N., Aizharikov, A. and Popov, A.I. (2021b), "Influence of productive Impurities (Cd, Na, O) on the Properties of the Cu2ZnSnS4 Absorber of Model Solar Cells", *Latv. J. Phys. Tech. Sci.*, **58**, 13-23. https://doi.org/10.2478/lpts-2021-0042

Sinko, M.R., de la Barrera, S.C., Lanes, O., Watanabe, K., Taniguchi, T., Tan, S.S., Pekker, D., Hatridge, M. and Hunt, B.M. (2021), "Superconducting contact and quantum interference between two-dimensional van der Waals and three-dimensional conventional superconductors", *Phys. Rev. Mater.*, **5**, 014001. https://doi.org/10.1103/PhysRevMaterials.5.014001

Tsuppayakorn-aek, P., Pluengphon, P., Phansuke, P., Inceesungvorn, B., Busayaporn, W., Kaewtubtim, P. and Bovornratanaraks, T. (2021), "Effect of substitution on the superconducting phase of transition metal dichalcogenide Nb(SexS1-x)2 van der Waals layered structure", *Sci. Rep.*, **11**, 15215. https://doi.org/10.1038/s41598-021-94000-2

Wang, H.W., Kumar, A., Dai, S.Y., Lin, X., Jacob, Z.B., Oh, S.H., Menon, V., Narimanov, E., Kim, Y.D., Wang, J.P., Avouris, P., Moreno, L.M., Caldwell, J. and Low, T. (2024), "Planar hyperbolic polaritons in 2D van der Waals materials", *Nature Commun.*, **15**, 69. https://doi.org/10.1038/s41467-023-43992-8

Wang, P.Q., Jia, C.C., Huang, Y. and Duan, X.F. (2021), “Van der Waals Heterostructures by Design: From 1D and 2D to 3D”, *Matter*, **4**(2), 552-581. https://doi.org/10.1016/j.matt.2020.12.015

Xiang, R., Inoue T., Zheng Y., Kumamoto A., Qian Y., Sato Y. et al. (2020), “One-dimensional van der Waals heterostructures”, *Science*, **367**(6477), 537-542. https://doi.org/10.1126/science.aaz2570

Xie, Y., Jiang, N.N., Han, W., Wang, S.F., Chen, L.Y., Jin, X.W., Chen, Z.Y., Xiao, X.S., Zhou, Z.X. and Song, Y.L. (2024), “Electric field tunable electronic structures and ultrahigh power conversion efficiency of BC6N/MoSe2 van der Waals heterostructure: A promising material for high-efficiency solar cell applications”, *J. Phys. Chem. Solids*, **192**, 112067. https://doi.org/10.1016/j.jpcs.2024.112067

Yang, W., Cao, Y., Han, J., Lin, X., Wang, X., Wei, G., Lv, C., Bournel, A. and Zhao, W. (2021), “Spin-filter induced large magnetoresistance in 2D van der Waals magnetic tunnel junctions”, *Nanoscale*, **13**(2), 862-868. https://doi.org/10.1039/d0nr07290g

Yin, YH., Cao, G.H., Fu, L.G., Wei, Z.F., Li, H.F., Wu, P.P., Li, M., Zong, H.T., Yan, L.L. and Zhang, B.Q. (2021), “Functionalized multi-walled carbon nanotubes with strong fluorescence emission”, *J. Alloy. Compd.*, **854**, 157016. https://doi.org/10.1016/j.jallcom.2020.157016

Zhu, J., Chen, X., Shang, W., Ning, J., Wang, D., Zhang, J. and Hao, Y. (2021), “Van der Waals contact between 2D magnetic VSe2 and transition metals and demonstration of high-performance spin-field-effect transistors”, *Sci. China Mater.*, **64**, 2786-2794. https://doi.org/10.1007/s40843-021-1657-9

CC